Retrograde Melanopsin Signaling Increases With Age in Retinal Degenerate Mice Lacking Rods and the Majority of Cones

Ma'ayan Semo,[1] Peter Coffey,[1,2] Carlos Gias,[1] and Anthony Vugler[1]

[1]Department of Ocular Biology and Therapeutics, UCL-Institute of Ophthalmology, London, United Kingdom
[2]Neuroscience Research Institute, University of California-Santa Barbara, Santa Barbara, California, United States

Correspondence: Anthony Vugler, Department of Ocular Biology and Therapeutics, UCL-Institute of Ophthalmology, 11-43 Bath Street, London, UK; a.vugler@ucl.ac.uk.

Submitted: July 2, 2015
Accepted: December 8, 2015

Citation: Semo M, Coffey P, Gias C, Vugler A. Retrograde melanopsin signaling increases with age in retinal degenerate mice lacking rods and the majority of cones. *Invest Ophthalmol Vis Sci*. 2016;57:115–125. DOI:10.1167/iovs.15-17609

Purpose. Following on from reports of retrograde retinal signaling in mice, we sought to investigate the influence of age and retinal location on this phenomenon using mice that lack rods and the majority of cones.

Methods. We used functional anatomy for c-fos (Fos) and tyrosine hydroxylase (TH) to measure light-driven activation of dopamine neurons along a dorsal–ventral transect in C3H/He wild-type and rodless-coneless *rd/rd cl* (*rdcl*) mice aged 3, 5, and >14 months. A parallel series of retinae from 3-month-old mice was also stained for cone opsins and melanopsin.

Results. Analysis by confocal microscopy revealed light-driven Fos activation in TH cells residing in the middorsal retina of the youngest *rdcl* mice. This region was largely devoid of residual cones but contained a large number of intrinsically photosensitive retinal ganglion cells (ipRGCs) and the highest density of melanopsin neurites. With advancing age, there was a paradoxical increase in retrograde signaling from ~3% Fos-positive (Fos+) TH cells at 3 months to ~36% in *rdcl* mice >14 months. This increased activation occurred in more central and peripheral retinal regions.

Conclusions. Our data provide new insights into the anatomy and plasticity of retrograde melanopsin signaling in mice with severe rod/cone dystrophy. The increased retrograde signaling we detect may result from either an increased potency of melanopsin signaling with advancing age and/or postsynaptic modification to dopaminergic neurons.

Keywords: melanopsin, tyrosine hydroxylase, blue cones, cfos

The mammalian retina transduces light into electrical signals using rods, cones, and melanopsin-expressing intrinsically photosensitive retinal ganglion cells (ipRGCs). While it is well established that visual information flows from rods/cones to RGCs, recent evidence also supports the existence of melanopsin-driven intraretinal signaling,[1–3] with a distinct retrograde signaling pathway between ipRGCs and tyrosine hydroxylase (TH)-positive retinal dopamine neurons.[4–6]

Melanopsin and dopaminergic neurites form an interwoven plexus in sublamina 1 (OFF subdivision) of the inner plexiform layer (IPL-1),[7] with convergent evidence supporting neurotransmission from dopamine neurons to M1-type ipRGC.[8–11] Although both ipRGCs and dopamine neurons receive excitatory input from ON bipolar cells,[12,13] targeted electrophysiology in TH reporter mice has also revealed a subpopulation of retinal dopamine neurons (~21%) that maintain sustained responses to light in the presence of L-AP4, an mGluR6 receptor agonist that blocks signaling between rods/cones and ON-bipolar cells.[4,14] These sustained light responses are retained in *rd1* mice with outer retinal degeneration from 1 to 2 months of age,[4,15] are absent from wild-type and *rd1* mice lacking melanopsin (also 1–2 months of age),[5,15] and appear to be mediated by AMPA-type glutamate receptors.[5] Although the nature of this synaptic interaction is unclear, it may involve recurrent axon collaterals from M1-type ipRGCs.[16]

Light-driven activation of retinal dopamine neurons can also be assessed using immunofluorescent double labeling for c-fos (Fos) and TH.[17] In *rd1* mice aged 4 to 13 months, it has been reported that 21% of TH cells become Fos+ following light exposure.[4] However, no light-driven dopamine release or TH cell Fos activation could be detected in *rdcl* mice aged 2 to 4 months.[18] The *rdcl* mouse has been used extensively to study the melanopsin system,[1,19,20] as this model is largely devoid of cones,[20,21] which can persist and function in adult *rd1* mice.[22,23]

Given the discrepancy between anatomical studies of TH cell activation in retinal degenerate mice,[4,18] the present study sought to re-examine the issue of TH cell activation in *rdcl* and congenic wild-type mice of different ages using spatially defined sampling of retinal whole mounts. In order to further understand any relationship between light-driven TH cell activation and surviving photoreceptors, a parallel series of retinae was also stained for cone opsins and melanopsin. Our data on TH cell activation in young versus old *rdcl* mice was originally presented as an ARVO abstract: Vugler AA, et al. *IOVS* 2010;51:ARVO E-Abstract 678.

Methods

Animal Husbandry

Animals used in this study were either wild-type C3H/He or C3H/He *rdcl* mice, which undergo a rapid degeneration of rods

and cones over the first 3 postnatal weeks.[20,24] Animals were housed under a 12-hour light, 12-hour dark cycle (on at 7 AM, off at 7 PM), with the presence of *cl* transgene confirmed by genotyping mice prior to experimentation. To do this, genomic DNA was extracted from ear punch samples, and PCR was carried out to check for the presence of the *cl* transgene using the primers FOR-GTACCACGGGACTAAACC and REV-ATACT-CATACATCGCATCTTG, which produce a 486-bp product if the *cl* transgene is present. Animal experiments adhered to both the ARVO Statement for the Use of Animals in Ophthalmic and Vision Research and UK Home Office regulations.

Functional Anatomy Using Fos Immunohistochemistry

Following overnight dark adaptation, mice were processed in counterbalanced groups between 8 and 11 AM, either light-adapted for 90 minutes (broadband white light, 250 μW/cm^2 at cage level, ~400 lux), or retained under dark-adapted conditions for 90 minutes. A total of 12 wild-type mice aged 3 to 15 months (90–450 days, $n = 6$ light-adapted and $n = 6$ dark-adapted) and 22 *rdcl* mice aged 3 to 19 months (90–571 days, $n = 13$ light-adapted and $n = 9$ dark-adapted) were perfused, and retinal whole mounts prepared as previously described to maintain orientation.[25,26] The light level used here is equivalent to $\sim 1 \times 10^{14}$ photons/cm^2/s (at 480 nm), which exceeds the threshold for melanopsin activation ($\sim 1 \times 10^{12}$ photons/cm^2/s) found in studies of the pupillary light reflex (PLR)[27] and is ~3-fold brighter than the light used to activate Fos in *rd* mice by Zhang and colleagues.[4]

Counterbalanced groups of retinae were processed for immunofluorescent double labeling with a cocktail of rabbit anti-Fos (1:5000, PC38; Merck Millipore, Temecula, CA, USA) and sheep anti-tyrosine hydroxylase (TH; 1:5000, AB1542; Chemicon Millipore, Temecula, CA, USA) as previously described.[25] One retina in each staining batch was processed in the absence of primary antibodies as a negative control.

Immunohistochemistry for Melanopsin and Cone Opsins in *rdcl* Mice

A separate group of *rdcl* mice ($n = 6$ aged 90–98 days) were perfused and their retinae double-labeled for either melanopsin and Brn3b ($n = 6$ retinae), or M-opsin and S-opsin ($n = 5$ retinae) using rabbit anti-melanopsin (1:5000, UF006; Advanced Targeting Systems, San Diego, CA, USA); goat anti-Brn3b (1:100, sc-31987; Santa Cruz Biotechnology, Dallas, TX, USA); rabbit anti-M/L opsin (1:5000, AB5405; Merck Millipore); and goat anti–S-opsin (1:500, sc-14363; Santa Cruz Biotechnology) as previously described.[25,26] A further three retinae from [$n = 3$] 14-month-old (430 days) *rdcl* mice were also stained for M/L opsin and S-opsin.

Analysis of Retinal Whole Mounts

Immunohistochemical staining was analyzed using a Zeiss LSM 510 confocal microscope and LSM software (Zeiss, Jena, Germany). For each retina double-labeled with TH and Fos, a series of confocal Z stacks (typically 12 nonoverlapping optical slices of <1 μm) were acquired through the IPL/inner nuclear layer (INL) at 6 equally spaced locations spanning the dorsal–ventral axis of midsagittal retina. These regions were labeled dorsal peripheral (DP), dorsal (D), dorsal central (DC), ventral central (VC), ventral (V), and ventral peripheral (VP) following a previous convention.[28] Each confocal region covered 576 × 576 μm, giving a total sampled area of 2 mm^2 per retina.

Confocal files were coded, and a single observer made all counts blind to the experimental conditions. The assessment of TH and Fos colocalization was made in three-dimensional (3D) confocal Z stacks following standardized contrast and brightness adjustments to optimize the signal in each staining batch. For each Z stack, total TH cell number was counted and an arrowhead positioned at the perimeter of each cell. The TH cells were then carefully assessed for Fos colocalization by turning off the TH channel and assessing the distribution of Fos. Tyrosine hydroxylase cells were deemed Fos+ if Fos immunoreactivity was asymmetrically localized toward the nuclear region of the cell as described previously.[18,29] Tyrosine hydroxylase cells with diffuse cytosolic Fos signal, which extended to the cellular perimeter, were not counted as positive. The approach of analyzing TH+Fos colocalization in 3D Z stacks (as opposed to 2D projections) allowed the accurate determination of Fos label within TH cells, eliminating the risk of false positives from Fos in adjacent non-TH cells.

For *rdcl* retinae double-labeled with cone opsin antibodies, the entire population of M-opsin and S-opsin cones was counted at low magnification in each retinal quadrant using a Leica epifluorescent microscope (Leica, Milton Keynes, UK). For *rdcl* retinae double-labeled with melanopsin and Brn3b, staining was sampled using the same protocol as described above for the TH+Fos. At each sampling location, Z stacks were acquired encompassing the entire inner retina (RGC, IPL, and INL), and the total number of ipRGC somas was counted in both INL and RGC layers. The INL contains displaced ipRGCs (d-ipRGCs), and these were further analyzed for colocaliztion with Brn3b by removing the melanopsin-stained channel. As we counted both weakly and strongly stained somas, our data will essentially include all M1 and M2 ipRGCs but may also include M3 and possibly even M4 subtypes, which are all detectable using melanopsin immunohistochemistry.[30,31]

In order to make an objective assessment of melanopsin-positive neurite staining in IPL-1, a restricted projection was made from each Z stack to encompass only the region bordering INL/IPL. The total area of melanopsin neurites was then automatically quantified using a program written in MATLAB (R2010a; Natick, MA, USA; see Supplementary Methods). Retinal images were first filtered and enhanced using a combination of opening-by-reconstruction and application of the Frangi filter that enhances elongated structures.[32] A normalized threshold was then applied to the resulting image in order to identify those pixels that most likely constituted neurites. The skeleton of neurites was then identified using the skeletonization morphologic operation followed by pruning. Finally, only those neurites with a length > 20 pixels were considered for quantification. This procedure was performed using either a low-normalized threshold, which reliably identified all neurites (both weakly and strongly stained) or a high-normalized threshold, which identified the most intensely stained dendrites of M1-type ipRGCs.

Statistical Analysis

Data were analyzed in both percentage and cell count (cells/mm^2) form using GraphPad Prism software (GraphPad Software, San Diego, CA, USA) and assessed for normality by plotting residuals with QQPlot in R (version 3.1.2; The R Foundation for Statistical Computing, Vienna, Austria). Percentage data were nonnormally distributed and analyzed using 2-tailed Mann-Whitney *U* tests, or Kruskal-Wallis tests followed by Dunn's post hoc comparisons. The light versus dark comparisons were also made using nonparametric statistics because dark data were also nonnormally distributed. All remaining cell count data (from light-treated animals and S-opsin cones), once transformed $Y = \sqrt{(Y + 0.5)}$, were normally distributed and analyzed by 2-way or 1-way ANOVA followed by post hoc Bonferroni's multiple comparison tests. Melanopsin

Investigative Ophthalmology & Visual Science

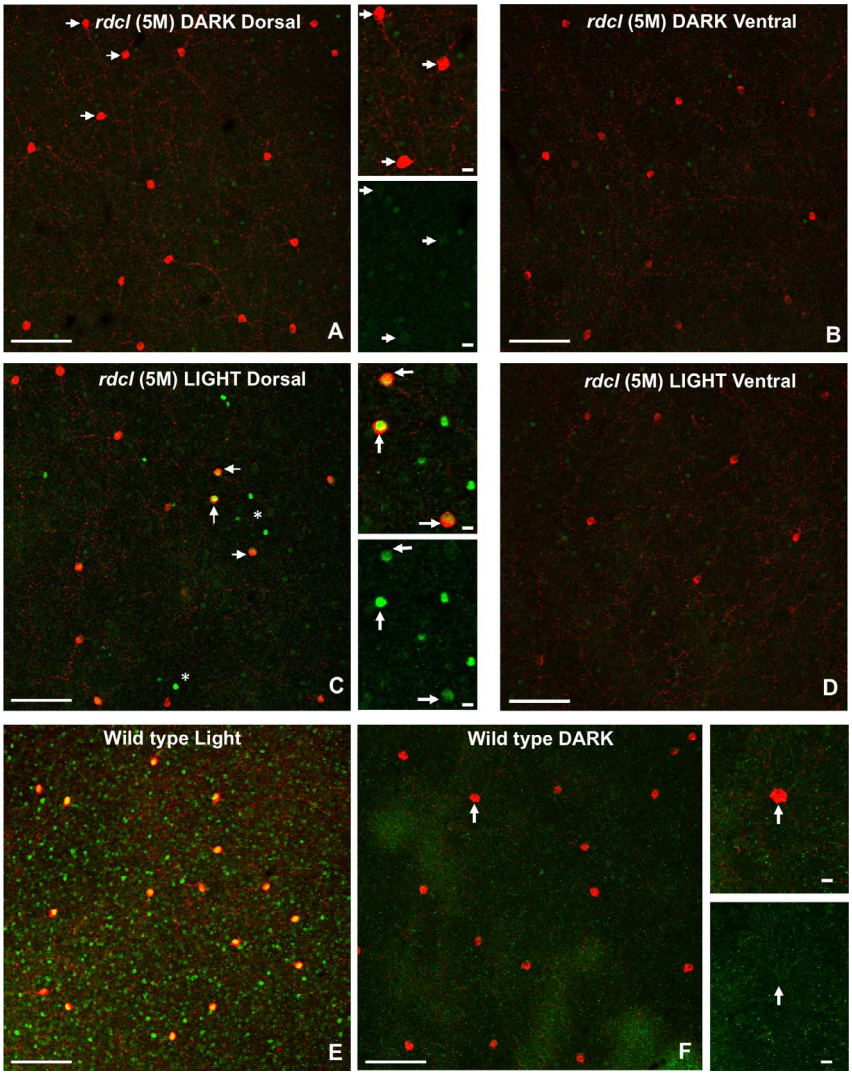

Figure 1. The Fos staining in TH cells from dark-adapted 5-month *rdcl* mice was diffuse, with an absence of nuclear localization in both the dorsal (**A**) and ventral (**B**) retina. Light-driven Fos activation (*yellow*) in TH neurons (*red*) was restricted to the dorsal retina in age-matched 5-month *rdcl* mice (compare [**C**, **D**]). Tyrosine hydroxylase neurons highlighted by *arrow*s in (**A**) and (**C**) are shown at higher magnification to the *right* of each image (merged and green-only channel). *Asterisks* in (**C**) indicate light-induced Fos (*green*) in non-TH cells. Examples of light-driven and dark-adapted Fos staining in the wild-type retina are shown *below* in (**E**) and (**F**), respectively. The TH neuron highlighted by an *arrow* in (**F**) is shown at higher magnification to the *right*. *Scale bars*: low magnification, 100 μm (**A**–**F**); high magnification, 10 μm (**A**, **C**, **F**).

neurite data were analyzed by 2-way ANOVA and Bonferroni's multiple comparison tests.

Results

Light-Driven TH Cell Activation in Wild-Type and *rdcl* Mice

Under dark-adapted conditions, TH cells from both *rdcl* and wild-type mice exhibited weak/diffuse cytosolic Fos (Figs. 1A, 1B, 1F), with only occasional evidence of nuclear Fos (Table). As shown in Figures 1C and 1D, we found clear evidence of light-driven nuclear Fos in TH cells from dorsal retina of 5-month-old *rdcl* mice. As previously described,[18] this technique also produced an almost total light-driven Fos activation of TH cells in wild-type mice, with between 93% and 100% of TH cells appearing Fos+ following light exposure, depending on retinal region (Figs. 1E, 1F, 2D). The Fos+ TH cells in light-adapted retinae were strongly labeled for TH and ~12 to 15 μm in diameter, corresponding to the type 1 TH-positive dopaminergic neurons reported by others.[33,34]

Overall, when all ages of *rdcl* mice were analyzed collectively, we detected a significant light-driven activation of TH cells in the *rdcl* retina, from a mean of 0.46 ± 0.28 (SEM) Fos+ TH cells/mm^2 (n = 13 retinae from 9 animals aged 3 to >14 months) in dark-adapted mice to 6.69 ± 1.14 Fos+ TH cells/mm^2 (n = 21 retinae from 13 animals aged 3 to >14 months) in light-adapted mice ($P < 0.0001$ by 2-tailed Mann-Whitney U test). As shown in the Table, animals were further subdivided on the basis of age into three separate groups: 3, 5, and >14 months (420–571 days), with each retina sampled at six different dorsal–ventral positions (illustrated in Fig. 2A). Analysis of Fos+ TH cells in *rdcl* mice at these different ages only revealed a significant effect of light in *rdcl* mice >14 months old ($P < 0.001$ by 2-tailed Mann-Whitney U test). This was due to both a higher number (Table) and higher percentage (Fig. 2B) of Fos+ TH cells in light-adapted *rdcl* mice with advancing age. In addition to light-driven TH cell

Table. Average Density of Fos+ TH Cells Taken From the Six Sampling Regions in Light-Adapted and Dark-Adapted C3H/He Wild-Type and *rdcl* Mice

Mouse	Age, mo	Fos+ TH in Light, Mean ± SEM Cells/mm²	*n*	Fos+ TH in Dark, Mean ± SEM Cells/mm²	*n*
Wild-type	3	32.33 ± 2.04	5(3)	0.00 ± 0.00‡	5(3)
Wild-type	>14	31.43 ± 0.79*	5(3)	0.20 ± 0.12	5(3)
rdcl	3	2.51 ± 1.25	5(3)	0.20 ± 0.20	5(3)
rdcl	5	4.02 ± 0.94	8(5)	0.00 ± 0.00‡	2(2)
rdcl	>14	11.99 ± 1.33†	8(5)	0.84 ± 0.56	6(4)

n, retinae sampled per group, with number of mice used in parentheses.

* $P < 0.01$ by Mann-Whitney *U* test.

† $P < 0.001$ by Mann-Whitney *U* test.

‡ Statistical analysis was not conducted where dark counts were all 0.

activation, the regional density of TH cells was also recorded in *rdcl* and wild-type mice (Fig. 3).

As shown in Figure 2, the response of TH cells to light in *rdcl* mice was very much reduced compared to that seen in the light-adapted wild-type retina. This level of light activation ranged from ~3% Fos+ TH cells at 3 months to ~36% in *rdcl* mice >14 months (Fig. 2B, $P < 0.01$). In the youngest *rdcl* mice, this TH cell activation was spatially discrete, with Fos+ TH cells being largely restricted to the dorsal retina at 3 months, peaking in sample region D, and being completely absent in ventral retinal regions V and VP (Figs. 2A, 2C, 2E). Kruskal-Wallis analysis of the regional light versus dark data for 3-month-old *rdcl* mice revealed a significant difference across regions ($P < 0.05$), with post hoc tests confirming that light-driven TH cell activation was restricted to retinal region D ($P < 0.05$).

Further analysis in *rdcl* mice aged 3, 5, and >14 months showed a significant difference in the regional percentage data ($P < 0.0001$ Kruskal-Wallis test), with Dunn's post hoc tests revealing significant increases in Fos+ TH cells at regions DC and VC of the oldest *rdcl* mice (Fig. 2C). In light-adapted *rdcl* mice aged >14 months, TH cell activation peaked in region DC, where ~63% of TH cells were Fos+. A similar pattern can be seen in Figure 2E, where 2-way ANOVA of count data confirmed a significant effect of region $P < 0.0001$ ($F_{5,66} = 3.593$), age $P < 0.0001$ ($F_{1,66} = 16.16$), and an interaction between these two factors $P < 0.05$ ($F_{5,66} = 0.8825$), with post hoc Bonferroni comparison tests showing more TH cell activation in the DP, DC, and VC regions of *rdcl* mice aged >14 months (Fig. 2E). In contrast, we could detect no significant impact of age or retinal region on either the proportion (Fig. 2D) or number (Fig. 2F) of Fos+ TH cells in wild-type mice.

Representative images of light-driven TH cell activation from young and old *rdcl* mice are shown in Figures 4 and 5, respectively. In addition to light-driven TH cell activation, we also found strong light-driven Fos in a small population of TH-negative INL neurons (asterisks in Figs. 1, 4, 5). Quantification of light-adapted 3-month *rdcl* retinae ($n = 5$) revealed that the mean number (±SEM) of these Fos+ TH-negative cells per mm² varied by retinal region as follows: DP 4.01 ± 1.27; D 16.06 ± 2.65; DC 10.55 ± 1.3; VC 2.51 ± 0.93; V 2.02 ± 0.99; VP 2.51 ± 0.93. There were also discrete clusters of smaller Fos+ cells in both light- and dark-adapted *rdcl* retina. These clusters of Fos activity were most common in 3-month-old *rdcl* mice (typically 1–4 clusters per image, see small arrows in Fig. 4), but were also occasionally found in older *rdcl* mice and dark-adapted wild-type mice >14 months (data not shown). We suggest that these Fos+ clusters may reflect the bursts of spontaneous neural activity that occur in response to ongoing retinal degeneration.[35,36]

TH Cell Distribution in Aging and Retinal Degeneration

One-way ANOVA of overall TH cell numbers counted in wild-types and *rdcl* revealed significant differences between the groups ($P < 0.0001$). In wild-type mice, the density of TH cells remained stable with advancing age (29.97 ± 1.55 cells/mm² at 3 months versus 32.58 ± 0.73 in mice >14 months), while in *rdcl* mice we detected a small but significant decline (37.05 ± 0.71 TH cells/mm² at 3 months, 35.14 ± 0.52 at 5 months, and 32.09 ± 0.81 in mice >14 months ($P < 0.01$, Bonferroni's multiple comparison test). Interestingly, we found that the 3-month-old *rdcl* retina has a significantly higher density of TH cells than the age-matched wild-type ($P < 0.001$, Bonferroni's multiple comparison test), a finding that may reflect slower rates of eye/retinal growth in rodent models of outer retinal degeneration.[37,38] By 2-way ANOVA we also found a significant effect of age $P < 0.001$ ($F_{1,132} = 11.98$) and region $P < 0.0001$ ($F_{5,132} = 7.481$) and an interaction between these two factors ($P < 0.05$, $F_{5,132} = 2.953$) in *rdcl* mice (Fig. 3A). As indicated in Figure 3A, post hoc tests revealed a significant reduction of TH cells in region V of *rdcl* mice aged >14 months. This finding most likely reflects neovascular-induced pathology in the ventral retina of retinal degenerate mice.[39,40] Analysis by 2-way ANOVA also revealed a significant effect of region $P < 0.0001$ ($F_{5,108} = 6.088$) but not age (no interaction) in wild-type mice (Fig. 3B).

Photoreceptor Survival and Spatial Distribution

In order to further understand the relationship between light-driven TH cell activation and surviving photoreceptors, we examined both residual cone numbers in *rdcl* mice and the distribution of melanopsin-positive ipRGC somas/neurites. The latter was done in both *rdcl* and wild-type mice in order to determine any regional specializations, which may correlate with the dorsal–ventral differences in retrograde signaling identified by functional anatomy.

Cone Survival in *rdcl* Mice

In *rdcl* mice, diphtheria toxin mediates cone death in M-opsin expressing cones.[20,24] Consistent with this, we found a negligible number of M-opsin cones in 3-month *rdcl* mice (0–4 per retina). However, primordial blue cones, which express only S-opsin,[41] are not directly targeted in *rdcl* mice and have been noted to survive in small numbers ventrally.[21] As shown in Figure 6, we also found a significant number of residual S-opsin cones, which predominated in ventral–nasal retina of 3-month-old *rdcl* mice (1-way ANOVA $P < 0.0001$), post hoc comparisons showing that all regions are significantly different from each other ($P < 0.05$), apart from the dorsal–temporal versus dorsal–nasal regions ($P > 0.05$). This shows that primordial blue cones are not evenly distributed across the mouse retina as previously thought [41] and instead appear to be located in ventral–nasal retina, similar to the distribution of total S-opsin staining in this species.[42] We were also able to stain three retinae from 14-month-old *rdcl* mice and found only 10 to 12 S-opsin–positive cones per retina (0.7 ± 0.3 cones in the dorsal hemisphere and 10.3 ± 0.9 cones in ventral hemisphere).

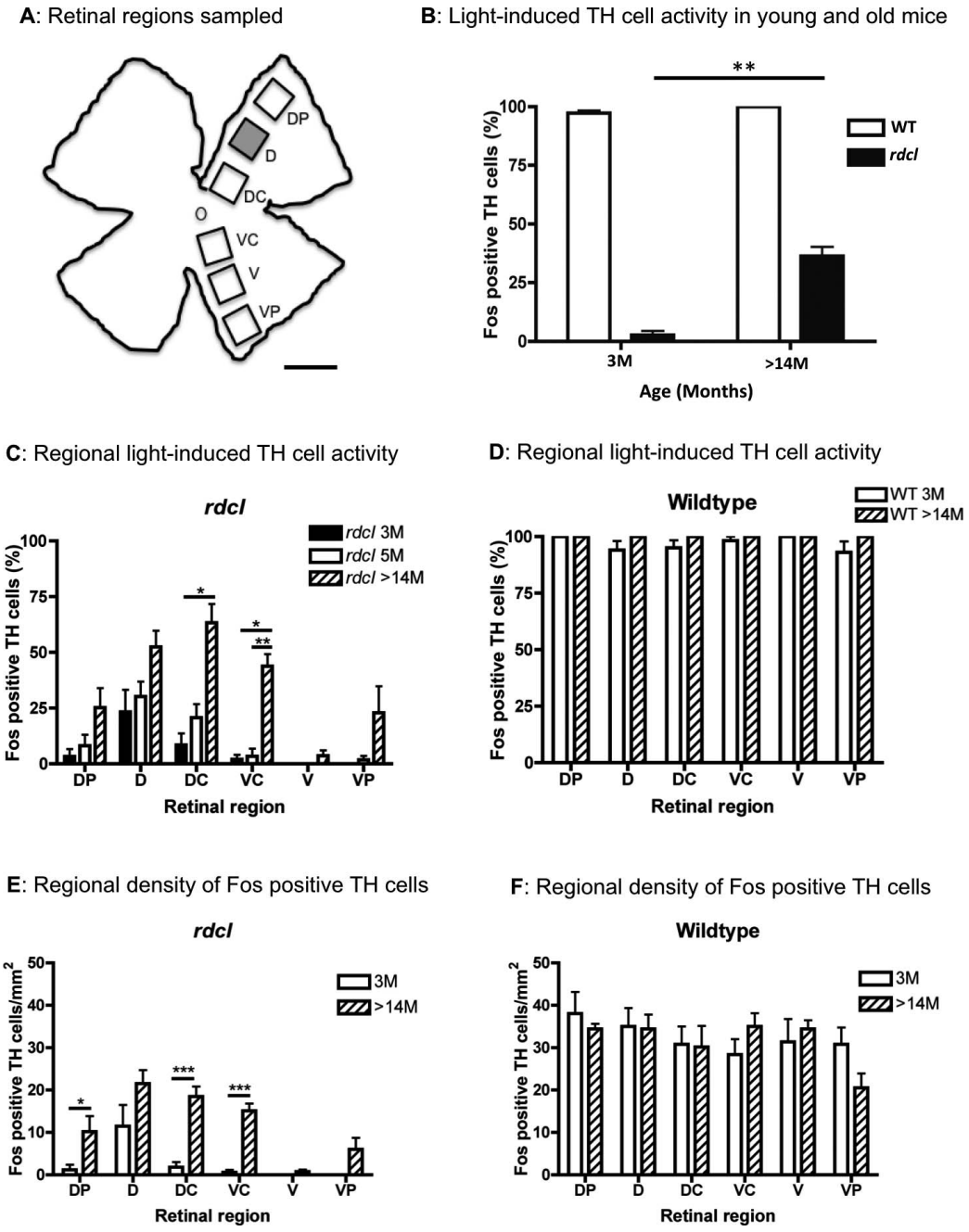

FIGURE 2. Retrograde signaling increases with age in *rdcl* mice. The retinal sampling regions used are illustrated in (**A**), with position D highlighted in *gray* to indicate the peak region of light-driven TH cell activation in younger (3 and 5 months) *rdcl* mice. (**B**–**D**) Proportion data with a clear increase in light-activated (Fos+) TH cells in *rdcl* mice >14 months (**B**). This increase occurred at most retinal regions analyzed in the oldest mice, with statistically significant differences in central retina (**C**). In contrast to *rdcl* mice, wild-type animals showed consistently high proportions of light-driven TH cell activation across all sampling regions regardless of age (**D**). The regional density of Fos+ TH cells (in cells/mm^2) is also plotted for *rdcl* (**E**) and wild-type (**F**) mice, where Fos+ TH cells are elevated across the retina in *rdcl* mice >14 months of age, with significant differences in regions DP, DC, and VC (**E**), but not in wild-type mice (**F**). Analysis by Mann-Whitney *U* test (**B**), Kruskal-Wallis with Dunn's multiple comparison (**C**), and 2-way ANOVA with post hoc Bonferroni comparisons (**E**, **F**). $^*P < 0.05$, $^{**}P < 0.01$, $^{***}P < 0.001$. *Scale bar*: 1 mm (**A**).

Distribution of ipRGCs and Melanopsin-Positive Neurites

Two-way ANOVA of ipRGCs in the RGC layer of 3-month-old mice revealed a significant regional difference in soma density in both wild-type and *rdcl* ($F_{5,60} = 29.34$, $P < 0.0001$), with the majority of ipRGCs being present in dorsal retina (Fig. 7A). We also found a significant effect of degeneration, with a slightly lower density of ipRGCs in *rdcl* mice ($F_{1,60} = 4.381$, $P = 0.0406$). However, this difference was subtle, with post hoc tests not revealing any significant differences in soma density in any particular retinal region.

In terms of d-ipRGCs with somas in the INL, 2-way ANOVA revealed a striking effect of region ($F_{5,60} = 57.67$, $P < 0.0001$), with the vast majority of d-ipRGCs residing in dorsal retinal regions D and DC (Fig. 7B). There was no difference in the density of d-ipRGCs between wild-type and *rdcl* mice, with colocalization analysis revealing that ~36% of d-ipRGCs were

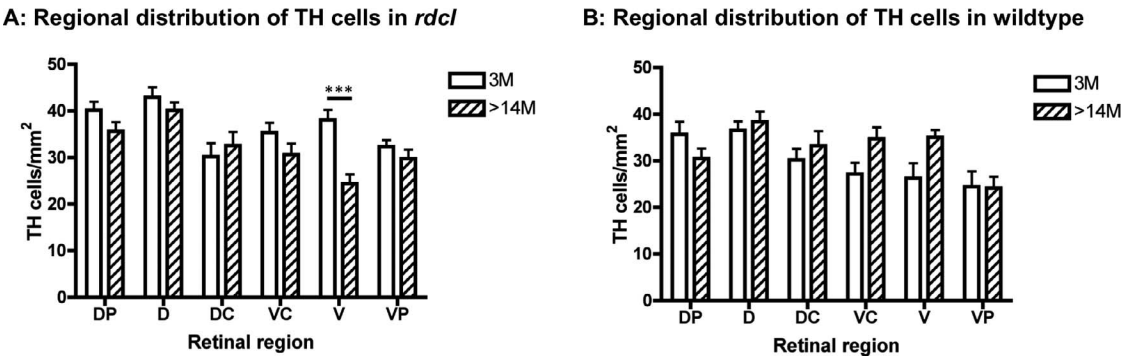

Figure 3. Regional density of TH cells in *rdcl* and wild-type mice. Graphs in (**A**) and (**B**) show the regional distribution of TH cells in young versus old *rdcl* and wild-type mice, respectively. Analysis by 2-way ANOVA and post hoc Bonferroni comparisons, $^{***}P < 0.001$.

positive for Brn3b (26 out of 72 cells). As previously reported, the Brn3b-positive population of d-ipRGCs was smaller and less intensely stained (small arrows in Fig. 7) and most likely represents a population of displaced M2 cells.[31]

The IPL-1 melanopsin plexus was assessed at both high threshold to measure strongly labeled M1 ipRGC dendrites and low threshold to include more weakly labeled dendrites/axons (collectively termed neurites). At high threshold (Fig. 8A), 2-way ANOVA found a significant effect of retinal region on M1 ipRGC dendrites ($F_{5,60} = 6.292$, $P < 0.0001$), with highest dendritic coverage in regions D, VC, and V, irrespective of retinal degeneration.

At low threshold, 2-way ANOVA found a significant effect of retinal region ($F_{5,60} = 28.48$, $P < 0.0001$), with a marked increase in coverage of neurites in the dorsal retina, peaking in region D (Fig. 8B). There was also a small but significant effect of degeneration on neurite coverage in the low-threshold group ($F_{1,60} = 4.488$, $P = 0.0383$), with fewer neurites in the *rdcl* retina. However, post hoc tests failed to find significance at any particular retinal location.

In order to quantify changes to neurites other than M1 dendrites, the high-threshold data were then subtracted from low-threshold data (Fig. 8C). Analysis of these data by 2-way ANOVA revealed significant effects of both retinal region ($F_{5,60} = 40.20$, $P < 0.0001$) and degeneration ($F_{1,60} = 8.486$, $P = 0.005$), with post hoc tests showing significantly fewer lightly stained neurites in region D of the *rdcl* retina ($P < 0.05$, Fig. 8C).

Discussion

Here we used functional anatomy to study the progression of retrograde signaling in *rdcl* mice that lack rods and the vast majority of cones. This signaling is initially localized to the middorsal retina in young mice but expands to encompass more central/peripheral regions with advancing age. In support of melanopsin driving this response in young *rdcl* mice, we also report a peak in the number of M1/M2-like d-ipRGC and melanopsin-positive neurites in middorsal retina, while the residual primordial blue cones predominate in ventral retina.

Given the small and localized light response reported here in younger *rdcl* mice, it is easy to see how this could have been missed in the previous study by Cameron et al.,[18] where

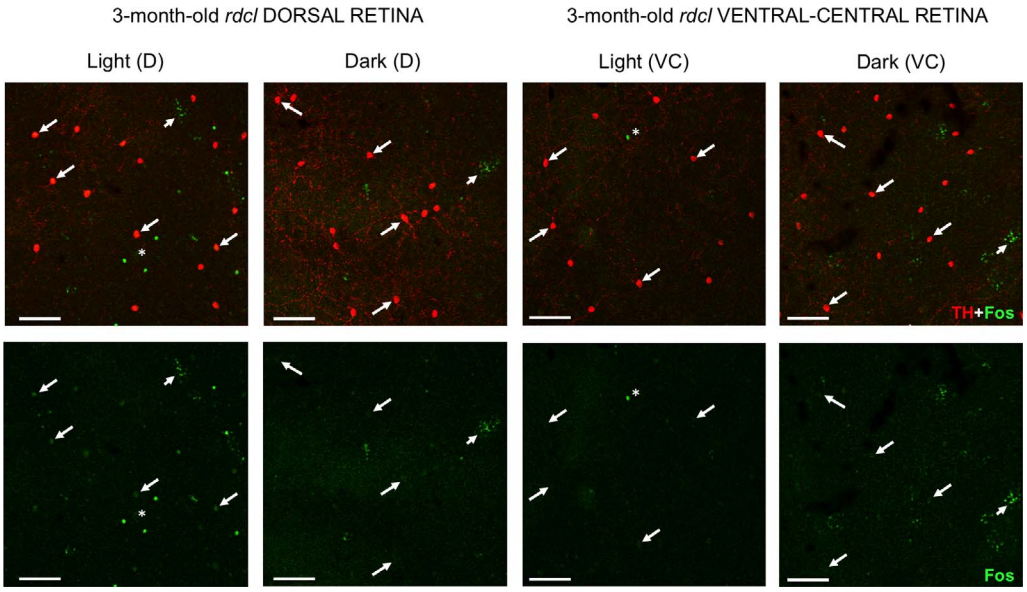

Figure 4. Representative examples of TH (*red*) and Fos (*green*) labeling from the dorsal (region D) and ventral–central (VC) retina of light-adapted (Light) and dark-adapted (Dark) *rdcl* mice aged 3 months. *Long arrows* point to TH cells and *short arrows* point to clusters of spontaneous Fos activity. For comparison, the separated green channel is shown *below* each merged image, where the *arrows* correspond to those *above*. *Asterisks* indicate additional light-induced Fos in non-TH cells. *Scale bars*: 100 μm.

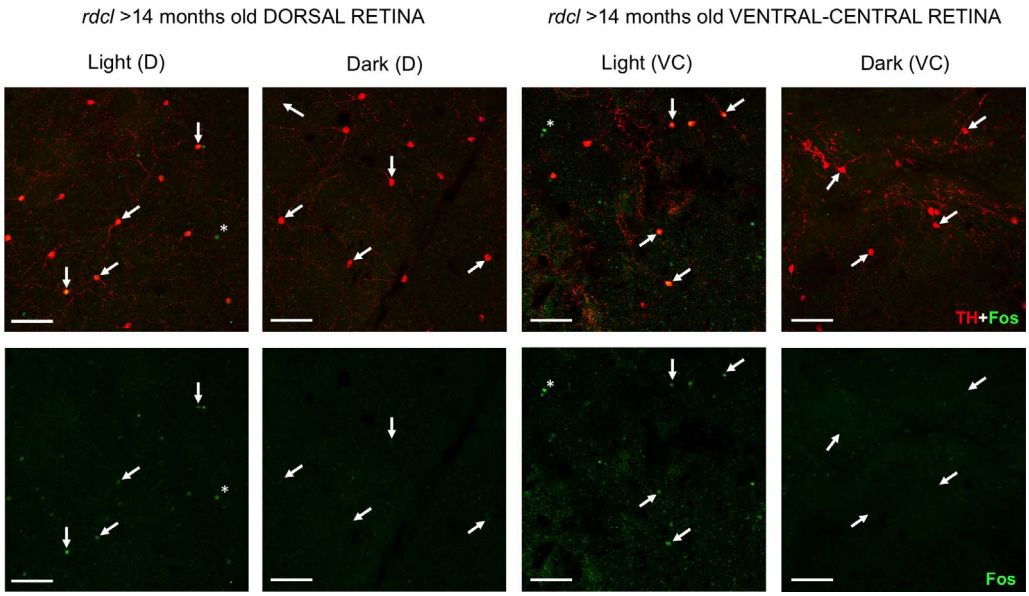

FIGURE 5. Representative examples of TH (*red*) and Fos (*green*) labeling from dorsal (region D) and ventral–central (VC) retina of light-adapted (Light) and dark-adapted (Dark) *rdcl* mice aged >14 months. The *arrows* identify TH cells in both the merged images (*top row*) and separated green channel *below*. *Asterisks* indicate additional light-induced Fos in non-TH cells. *Scale bars*: 100 μm.

analysis was restricted to 10 randomly selected TH cells per animal in tissue sections.[18] Our data support the anatomical findings of Zhang and colleagues[4] in *rd1* mice and suggest that they may have detected light-driven TH cell activation in sectioned material because of the aged component to their mouse cohort. Our findings are also consistent with reports of light-driven electrophysiological activity in TH cells from young (1–2 months old) *rd1* mice,[15] although the levels of TH cell activation we report here using functional anatomy may actually underestimate the degree to which retrograde melanopsin signaling operates in younger *rdcl* mice. This is because electrophysiological activity may need to reach a certain threshold in order to produce nuclear Fos signals in TH neurons. Our finding that the potency of melanopsin-driven retrograde signaling increases with age in *rdcl* mice is paradoxical, exciting, and consistent with complementary data from several previous studies.

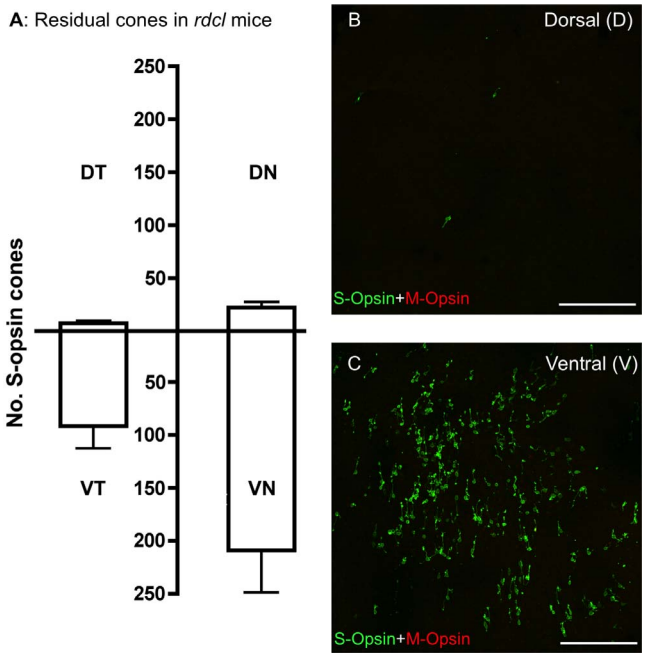

FIGURE 6. The retina of adult (3-month) *rdcl* mice retains a significant number of primordial blue cones, expressing only S-opsin. (**A**) Residual S-opsin–positive cones predominate in ventral retina. (**B**, **C**) Representative images from the dorsal retina (region D) and ventral retina (region V), respectively. S-opsin staining is in *green* and M-opsin staining is in *red*. DN, dorsal–nasal; DT, dorsal–temporal; VN, ventral–nasal; VT, ventral–temporal. *Scale bars*: 200 μm.

The first of these is a study examining light-evoked dopamine metabolism in retinal degenerate (*rds*) mice, which was only able to find a small but significant light-evoked increase in retinal dopamine metabolism in the oldest (~1 year) animals studied.[43] During the preparation of this manuscript, we became aware of an electrophysiological study by Atkinson and colleagues,[15] reporting convergent evidence for increased light-driven TH cell activation in aging *rd1* mice. This took the form of increased firing frequency, peak amplitude, and reduced latency to peak in the light-activated TH neurons of *rd1* mice aged 6 to 7 months (relative to those aged 1–2 months) and was also interpreted as reflecting enhanced melanopsin signaling. Other evidence from our laboratory has also shown paradoxical increases in melanopsin-driven light avoidance behavior[44] and intrinsic pupillary light responses[40] with increasing age in retinal degenerate mice. Also, although ipRGC numbers decline in aged *rdcl* mice,[40] the consensual PLR, circadian response to light, and even the levels of retinal melanopsin gene expression in these animals remain stable during advanced aging.[19]

One possible explanation for the increased potency of the melanopsin-driven retrograde signaling we observe involves the retinal pigment epithelium (RPE). Both melanopsin expression and ipRGC function are severely compromised in *Rpe65*$^{-/-}$ mice,[45–47] and compromising RPE function in *rd* or *rdta* mice reduces ipRGC function (as measured by the PLR) in these animals.[47] As the outer retina degenerates in rodents, the INL reduces in thickness and ipRGCs move physically closer to the RPE, both away from and close to regions of vascular anastomosis.[19,39,48] It therefore seems plausible that as retinal degeneration progresses with age in *rdcl* mice, the retinal

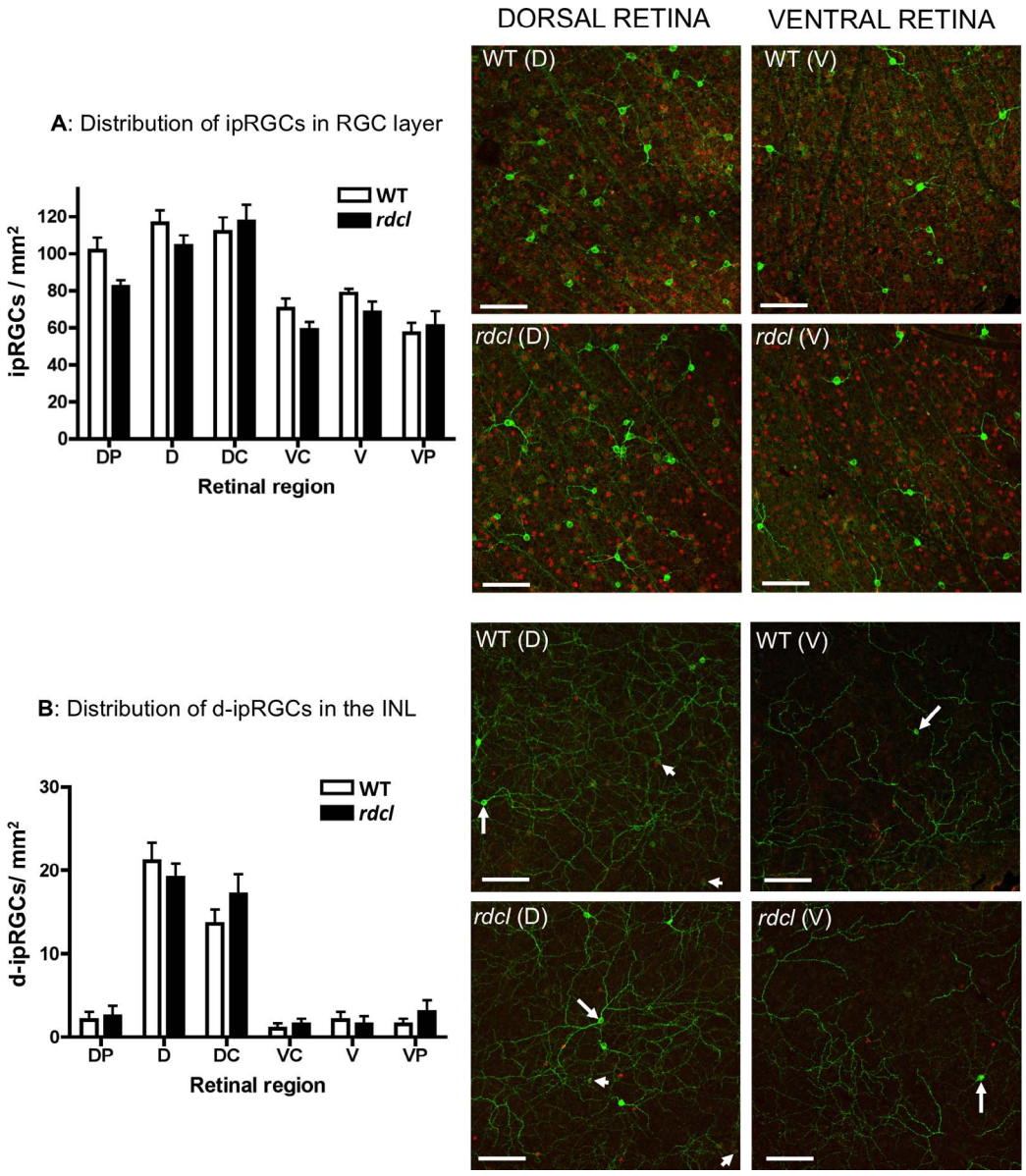

FIGURE 7. Melanopsin staining (*green*) in 3-month wild-type (WT) and *rdcl* mice reveals a peak in the distribution of ipRGCs in dorsal retina. Graph in (**A**) shows the distribution of ipRGCs in the retinal ganglion cell (RGC) layer, and graph in (**B**) shows the distribution of ipRGCs in the inner nuclear layer (INL). Representative confocal images from the dorsal (region D) and ventral (region V) retina of WT and *rdcl* mice are shown to the *right* of each graph. Retinae were double-labeled with Brn3B in order to identify the RGC layer. As indicated by *arrows*, the d-ipRGCs in the INL were either negative (*large arrows*) or positive (*small arrows*) for Brn3b. The confocal images adjacent to graph A were taken at the level of RGC layer, and those adjacent to graph B were taken at the IPL-INL border. Analysis by 2-way ANOVA revealed significant effects of region ($P < 0.0001$) and degeneration ($P = 0.0406$) in (**A**) and region ($P < 0.0001$) in (**B**). *Scale bars*: 100 μm.

chromophore available to support melanopsin function actually increases due to closer physical proximity between ipRGCs and the RPE. Alternative explanations could involve either an upregulation of melanopsin expression in individual ipRGCs or perhaps even an upregulation of visual cycle enzymes by surviving RPE cells with advancing age in retinal dystrophy. We consider it unlikely that the increased retrograde signaling with advancing age in *rdcl* mice results from a loss of S-cone input. This is because retrograde signaling increases with age in the dorsal retina but not region V of the ventral retina. Further work is needed to elucidate the mechanism(s) involved here.

Dopamine turnover in the retina is stimulated by light exposure and regulated by circadian time.[49,50] This results in elevated levels of dopamine release during daylight hours, during which dopamine enriches light-adapted vision by modulating retinal circuits to enhance cone signaling, contrast detection, and visual acuity.[51,52] Dopamine also attenuates the intrinsic photocurrent of ipRGCs[11] and as such appears to promote light adaptation of all photoreceptive systems.

Although we were not able to examine retrograde signaling directly in wild-type mice using the TH-Fos method, our results in *rdcl* mice show that melanopsin-driven retrograde signaling appears strongest in middorsal retina. We found this region to contain a high concentration of ipRGCs, d-ipRGCs, and melanopsin-positive neurites in both *rdcl* and wild-type mice, which is consistent with a report of high RGC density just dorsal to the optic nerve in this

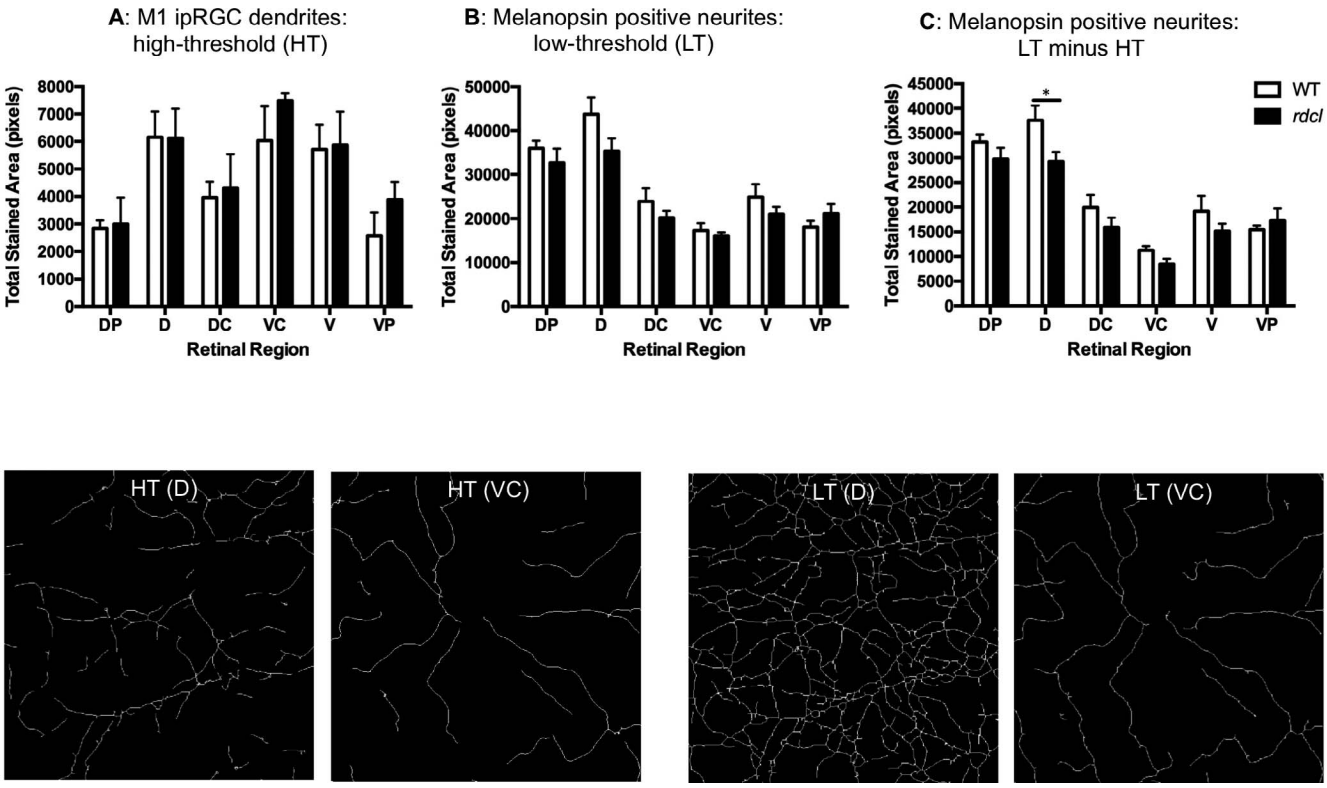

Figure 8. Regional quantification of melanopsin-positive neurites in the outer plexus (IPL-1) of 3-month wild-type (WT) and *rdcl* mice. Graph in (**A**) shows the total stained area (measured in pixels) for each retinal region when the threshold is set to high (to detect M1 ipRGC dendrites). This dendritic coverage is highest in regions D, VC, and V. Graph in (**B**) shows that when threshold is set to low (to detect both weakly and strongly stained neurites), coverage peaks in region D of dorsal retina. Neurites other than M1 dendrites were analyzed separately in graph (**C**) by subtracting the high- from low-threshold data. *Below the graphs* are representative high-threshold (HT) and low-threshold (LT) MATLAB images from regions D and VC. Analysis by 2-way ANOVA revealed significant effects of region ($P < 0.0001$) in (**A**) and region ($P < 0.0001$) plus degeneration ($P = 0.0383$) in (**B**). *$P < 0.05$ by post hoc Bonferroni analysis.

species.[53] This is the first time that the IPL-1 melanopsin plexus has been regionally analyzed in mice, and our data may reflect more axon collaterals and/or weakly stained ipRGC dendrites in the dorsal retina. Rather interestingly, there were fewer weakly stained neurites in middorsal retina of *rdcl* mice, a finding that opens the possibility for enhanced retrograde signaling in this region of wild-type mice compared to that seen in the *rdcl*. However, we were unable to address this issue further in the current study.

Our results for preferential ipRGC distribution in dorsal retina are consistent with two recent studies in this species[54,55] and the dorsal predominance of d-ipRGC we report for C3H/He wild-type mice similar to that reported for C57 wild-types.[55] In the primate retina, where between 40% and 60% of ipRGCs reside in the INL, there is also an increase in density of d-ipRGCs toward the fovea.[56,57] As such, d-ipRGCs (a proportion of which may actually be interneurons[55]) appear to be an integral part of the retinal circuitry specialized for high acuity vision. Based on the regional distribution of Fos+, TH-negative cells we detected here in *rdcl* mice, we suggest that these cells are most likely light-responsive d-ipRGCs. They may alternatively belong to other amacrine cell classes, as described previously for Fos+ cells in mice.[17]

In terms of a possible function for retrograde signaling in the dorsal retina of mice, we suggest that sustained melanopsin-driven activity in this dorsal region, emanating from d-ipRGCs and/or M1 ipRGCs (possibly via axon collaterals), may serve to augment dopaminergic signaling to enhance light adaptation, acuity, and contrast detection beyond that found in less specialized retinal regions. Additionally, because dopamine neurons are almost entirely interplexiform in mice[34] and signal with GABA,[51] the augmented release of GABA at IPL-1 and the outer plexiform layer may also enhance vision. The high density of ipRGCs and melanopsin neurites we report here in the dorsal retina of mice is consistent with recently proposed roles for melanopsin in contrast sensitivity, acuity, and light adaptation.[58,59]

In conclusion, our data provide new insights into the anatomy and plasticity of retrograde melanopsin signaling in mice with severe rod/cone dystrophy. Although we cannot presently rule out the possibility that postsynaptic modifications to dopaminergic neurons may underlie the increased retrograde signaling we detect here, another interpretation of our data is that the potency of melanopsin signaling increases with age in *rdcl* mice. This hypothesis is supported by previous observations of both increased light aversion behavior[44] and intrinsic pupil responses[40] with increasing age in *rdcl* mice.

Acknowledgments

We thank Rob Lucas from the University of Manchester for his generous gifts of C3h/He wild-type and *rdcl* mice.

A portion of this work has been published previously as an ARVO abstract: Vugler AA, et al. *IOVS* 2010;51:ARVO E-Abstract 678.

Supported by the London Project to Cure Blindness (PC) and a new investigator award from Fight for Sight, United Kingdom (AV).

Disclosure: **M. Semo**, None; **P. Coffey**, None; **C. Gias**, None; **A. Vugler**, None

References

1. Sekaran S, Foster RG, Lucas RJ, Hankins MW. Calcium imaging reveals a network of intrinsically light-sensitive inner-retinal neurons. *Curr Biol*. 2003;13:1290–1298.
2. Muller LP, Do MT, Yau KW, He S, Baldridge WH. Tracer coupling of intrinsically photosensitive retinal ganglion cells to amacrine cells in the mouse retina. *J Comp Neurol*. 2010;518: 4813–4824.
3. Reifler AN, Chervenak AP, Dolikian ME, et al. All spiking, sustained ON displaced amacrine cells receive gap-junction input from melanopsin ganglion cells. *Curr Biol*. 2015;25: 2763–2773.
4. Zhang DQ, Wong KY, Sollars PJ, Berson DM, Pickard GE, McMahon DG. Intraretinal signaling by ganglion cell photoreceptors to dopaminergic amacrine neurons. *Proc Natl Acad Sci U S A*. 2008;105:14181–14186.
5. Zhang DQ, Belenky MA, Sollars PJ, Pickard GE, McMahon DG. Melanopsin mediates retrograde visual signaling in the retina. *PLoS One*. 2012;7:e42647.
6. Dkhissi-Benyahya O, Coutanson C, Knoblauch K, et al. The absence of melanopsin alters retinal clock function and dopamine regulation by light. *Cell Mol Life Sci*. 2013;70: 3435–3447.
7. Vugler A. The relationship between retinal melanopsin and dopamine systems in the Royal College of Surgeons rat. *Program No 9778 2005 Neuroscience Meeting Planner*. Washington, DC: Society for Neuroscience; 2005. Available at: http://www.sfn.org/Annual-Meeting/Past-and-Future-Annual-Meetings/Abstract-Archive/Abstract-Archive-Detail?AbsYear=2005&AbsID=16010. Accessed November 16, 2005.
8. Vugler AA, Redgrave P, Semo M, Lawrence J, Greenwood J, Coffey PJ. Dopamine neurones form a discrete plexus with melanopsin cells in normal and degenerating retina. *Exp Neurol*. 2007;205:26–35.
9. Viney TJ, Balint K, Hillier D, et al. Local retinal circuits of melanopsin-containing ganglion cells identified by transsynaptic viral tracing. *Curr Biol*. 2007;17:981–988.
10. Ostergaard J, Hannibal J, Fahrenkrug J. Synaptic contact between melanopsin-containing retinal ganglion cells and rod bipolar cells. *Invest Ophthalmol Vis Sci*. 2007;48:3812–3820.
11. Van Hook MJ, Wong KY, Berson DM. Dopaminergic modulation of ganglion-cell photoreceptors in rat. *Eur J Neurosci*. 2012;35:507–518.
12. Dumitrescu ON, Pucci FG, Wong KY, Berson DM. Ectopic retinal ON bipolar cell synapses in the OFF inner plexiform layer: contacts with dopaminergic amacrine cells and melanopsin ganglion cells. *J Comp Neurol*. 2009;517:226–244.
13. Hoshi H, Liu WL, Massey SC, Mills SL. ON inputs to the OFF layer: bipolar cells that break the stratification rules of the retina. *J Neurosci*. 2009;29:8875–8883.
14. Zhang DQ, Zhou TR, McMahon DG. Functional heterogeneity of retinal dopaminergic neurons underlying their multiple roles in vision. *J Neurosci*. 2007;27:692–699.
15. Atkinson CL, Feng J, Zhang DQ. Functional integrity and modification of retinal dopaminergic neurons in the rd1 mutant mouse: roles of melanopsin and GABA. *J Neurophysiol*. 2013;109:1589–1599.
16. Joo HR, Peterson BB, Dacey DM, Hattar S, Chen SK. Recurrent axon collaterals of intrinsically photosensitive retinal ganglion cells. *Vis Neurosci*. 2013;30:175–182.
17. Hanzlicek BW, Peachey NS, Grimm C, Hagstrom SA, Ball SL. Probing inner retinal circuits in the rod pathway: a comparison of c-fos activation in mutant mice. *Vis Neurosci*. 2004;21: 873–881.
18. Cameron MA, Pozdeyev N, Vugler AA, Cooper H, Iuvone PM, Lucas RJ. Light regulation of retinal dopamine that is independent of melanopsin phototransduction. *Eur J Neurosci*. 2009;29:761–767.
19. Semo M, Peirson S, Lupi D, Lucas RJ, Jeffery G, Foster RG. Melanopsin retinal ganglion cells and the maintenance of circadian and pupillary responses to light in aged rodless/coneless (rd/rd cl) mice. *Eur J Neurosci*. 2003;17:1793–1801.
20. Lucas RJ, Freedman MS, Munoz M, Garcia-Fernandez JM, Foster RG. Regulation of the mammalian pineal by non-rod, non-cone, ocular photoreceptors. *Science*. 1999;284:505–507.
21. Brown TM, Tsujimura S, Allen AE, et al. Melanopsin-based brightness discrimination in mice and humans. *Curr Biol*. 2012;22:1134–1141.
22. Thyagarajan S, van Wyk M, Lehmann K, Lowel S, Feng G, Wassle H. Visual function in mice with photoreceptor degeneration and transgenic expression of channelrhodopsin 2 in ganglion cells. *J Neurosci*. 2010;30:8745–8758.
23. Carter-Dawson LD, LaVail MM, Sidman RL. Differential effect of the rd mutation on rods and cones in the mouse retina. *Invest Ophthalmol Vis Sci*. 1978;17:489–498.
24. Soucy E, Wang Y, Nirenberg S, Nathans J, Meister M. A novel signaling pathway from rod photoreceptors to ganglion cells in mammalian retina. *Neuron*. 1998;21:481–493.
25. Semo M, Gias C, Ahmado A, Vugler A. A role for the ciliary marginal zone in the melanopsin-dependent intrinsic pupillary light reflex. *Exp Eye Res*. 2014;119:8–18.
26. Vugler AA, Semo M, Joseph A, Jeffery G. Survival and remodeling of melanopsin cells during retinal dystrophy. *Vis Neurosci*. 2008;25:125–138.
27. Lucas RJ, Douglas RH, Foster RG. Characterization of an ocular photopigment capable of driving pupillary constriction in mice. *Nat Neurosci*. 2001;4:621–626.
28. Vugler AA, Redgrave P, Hewson-Stoate NJ, Greenwood J, Coffey PJ. Constant illumination causes spatially discrete dopamine depletion in the normal and degenerate retina. *J Chem Neuroanat*. 2007;33:9–22.
29. Roux P, Blanchard JM, Fernandez A, Lamb N, Jeanteur P, Piechaczyk M. Nuclear localization of c-Fos, but not v-Fos proteins, is controlled by extracellular signals. *Cell*. 1990;63: 341–351.
30. Estevez ME, Fogerson PM, Ilardi MC, et al. Form and function of the M4 cell, an intrinsically photosensitive retinal ganglion cell type contributing to geniculocortical vision. *J Neurosci*. 2012;32:13608–13620.
31. Jain V, Ravindran E, Dhingra NK. Differential expression of Brn3 transcription factors in intrinsically photosensitive retinal ganglion cells in mouse. *J Comp Neurol*. 2012;520: 742–755.
32. Frangi AF, Niessen WJ, Nederkoorn PJ, Bakker J, Mali WP, Viergever MA. Quantitative analysis of vascular morphology from 3D MR angiograms: in vitro and in vivo results. *Magn Reson Med*. 2001;45:311–322.
33. Zhang DQ, Stone JF, Zhou T, Ohta H, McMahon DG. Characterization of genetically labeled catecholamine neurons in the mouse retina. *Neuroreport*. 2004;15:1761–1765.
34. Wulle I, Schnitzer J. Distribution and morphology of tyrosine hydroxylase-immunoreactive neurons in the developing mouse retina. *Brain Res Dev Brain Res*. 1989;48:59–72.
35. Margolis DJ, Newkirk G, Euler T, Detwiler PB. Functional stability of retinal ganglion cells after degeneration-induced changes in synaptic input. *J Neurosci*. 2008;28:6526–6536.
36. Stasheff SF. Emergence of sustained spontaneous hyperactivity and temporary preservation of OFF responses in ganglion cells

Investigative Ophthalmology & Visual Science

of the retinal degeneration (rd1) mouse. *J Neurophysiol*. 2008; 99:1408–1421.

37. Park H, Tan CC, Faulkner A, et al. Retinal degeneration increases susceptibility to myopia in mice. *Mol Vis*. 2013;19: 2068–2079.
38. Semo M, Vugler AA, Jeffery G. Paradoxical opsin expressing cells in the inner retina that are augmented following retinal degeneration. *Eur J Neurosci*. 2007;25:2296–2306.
39. Wang S, Villegas-Perez MP, Vidal-Sanz M, Lund RD. Progressive optic axon dystrophy and vascuslar changes in rd mice. *Invest Ophthalmol Vis Sci*. 2000;41:537–545.
40. Vugler A, Semo M, Ortin-Martinez A, et al. A role for the outer retina in development of the intrinsic pupillary light reflex in mice. *Neuroscience*. 2015;286:60–78.
41. Haverkamp S, Wassle H, Duebel J, et al. The primordial, blue-cone color system of the mouse retina. *J Neurosci*. 2005;25: 5438–5445.
42. Ortin-Martinez A, Nadal-Nicolas FM, Jimenez-Lopez M, et al. Number and distribution of mouse retinal cone photoreceptors: differences between an albino (Swiss) and a pigmented (C57/BL6) strain. *PLoS One*. 2014;9:e102392.
43. Nir I, Iuvone PM. Alterations in light-evoked dopamine metabolism in dystrophic retinas of mutant rds mice. *Brain Res*. 1994;649:85–94.
44. Semo M, Gias C, Ahmado A, et al. Dissecting a role for melanopsin in behavioural light aversion reveals a response independent of conventional photoreception. *PLoS One*. 2010;5:e15009.
45. Fu Y, Zhong H, Wang MH, et al. Intrinsically photosensitive retinal ganglion cells detect light with a vitamin A-based photopigment, melanopsin. *Proc Natl Acad Sci U S A*. 2005; 102:10339–10344.
46. Doyle SE, Castrucci AM, McCall M, Provencio I, Menaker M. Nonvisual light responses in the Rpe65 knockout mouse: rod loss restores sensitivity to the melanopsin system. *Proc Natl Acad Sci U S A*. 2006;103:10432–10437.
47. Tu DC, Owens LA, Anderson L, et al. Inner retinal photoreception independent of the visual retinoid cycle. *Proc Natl Acad Sci U S A*. 2006;103:10426–10431.
48. Villegas-Perez MP, Lawrence JM, Vidal-Sanz M, Lavail MM, Lund RD. Ganglion cell loss in RCS rat retina: a result of compression of axons by contracting intraretinal vessels linked to the pigment epithelium. *J Comp Neurol*. 1998;392: 58–77.
49. Iuvone PM, Galli CL, Garrison-Gund CK, Neff NH. Light stimulates tyrosine hydroxylase activity and dopamine synthesis in retinal amacrine neurons. *Science*. 1978;202:901–902.
50. Doyle SE, McIvor WE, Menaker M. Circadian rhythmicity in dopamine content of mammalian retina: role of the photoreceptors. *J Neurochem*. 2002;83:211–219.
51. Witkovsky P. Dopamine and retinal function. *Doc Ophthalmol*. 2004;108:17–40.
52. Jackson CR, Ruan GX, Aseem F, et al. Retinal dopamine mediates multiple dimensions of light-adapted vision. *J Neurosci*. 2012;32:9359–9368.
53. Salinas-Navarro M, Jimenez-Lopez M, Valiente-Soriano FJ, et al. Retinal ganglion cell population in adult albino and pigmented mice: a computerized analysis of the entire population and its spatial distribution. *Vis Res*. 2009;49:637–647.
54. Hughes S, Watson TS, Foster RG, Peirson SN, Hankins MW. Nonuniform distribution and spectral tuning of photosensitive retinal ganglion cells of the mouse retina. *Curr Biol*. 2013;23: 1696–1701.
55. Valiente-Soriano FJ, Garcia-Ayuso D, Ortin-Martinez A, et al. Distribution of melanopsin positive neurons in pigmented and albino mice: evidence for melanopsin interneurons in the mouse retina. *Front Neuroanat*. 2014;8:131.
56. Dacey DM, Liao HW, Peterson BB, et al. Melanopsin-expressing ganglion cells in primate retina signal colour and irradiance and project to the LGN. *Nature*. 2005;433:749–754.
57. Jusuf PR, Lee SC, Hannibal J, Grunert U. Characterization and synaptic connectivity of melanopsin-containing ganglion cells in the primate retina. *Eur J Neurosci*. 2007;26:2906–2921.
58. Schmidt TM, Alam NM, Chen S, et al. A role for melanopsin in alpha retinal ganglion cells and contrast detection. *Neuron*. 2014;82:781–788.
59. Allen AE, Storchi R, Martial FP, et al. Melanopsin-driven light adaptation in mouse vision. *Curr Biol*. 2014;24:2481–2490.

Investigative Ophthalmology & Visual Science